How to cite: Angew. Chem. Int. Ed. 2023, e202314999
doi.org/10.1002/anie.202314999

Polyoxometalates Hot Paper

Hydrogenation Catalysis by Hydrogen Spillover on Platinum-Functionalized Heterogeneous Boronic Acid-Polyoxometalates

Shujun Li, Yubin Ma, Yue Zhao, Rongji Liu, Yupeng Zhao, Xusheng Dai, Nana Ma, Carsten Streb,* and Xuenian Chen**

Abstract: The activation of molecular hydrogen is a key process in catalysis. Here, we demonstrate how polyoxometalate (POM)-based heterogeneous compounds functionalized with Platinum particles activate H_2 by synergism between a hydrogen spillover mechanism and electron-proton transfer by the POM. This interplay facilitates the selective catalytic reduction of olefins and nitroarenes with high functional group tolerance. A family of polyoxotungstates covalently functionalized with boronic acids is reported. In the solid-state, the compounds are held together by non-covalent interactions (π–π stacking and hydrogen bonding). The resulting heterogeneous nanoscale particles form stable colloidal dispersions in acetonitrile and can be surface-functionalized with platinum nanoparticles by in situ photoreduction. The resulting materials show excellent catalytic activity in hydrogenation of olefins and nitrobenzene derivatives under mild conditions (1 bar H_2 and room temperature).

[*] Prof. Dr. S. Li, M. Sc. Y. Ma, Dr. Y. Zhao, Dr. X. Dai, Dr. N. Ma, Prof. Dr. X. Chen
Henan Key Laboratory of Boron Chemistry and Advanced Energy Materials, Key Laboratory of Green Chemical Media and Reactions, Ministry of Education, School of Chemistry and Chemical Engineering, Henan Normal University
Xinxiang, 453007 (China)
E-mail: lisj@htu.edu.cn

Prof. Dr. S. Li, Dr. R. Liu, M. Sc. Y. Zhao, Prof. Dr. C. Streb
Institute of Inorganic Chemistry I, Ulm University
Albert-Einstein-Allee 11, 89081 Ulm (Germany)

Dr. R. Liu, M. Sc. Y. Zhao, Prof. Dr. C. Streb
Department of Chemistry, Johannes Gutenberg University Mainz
Duesbergweg 10–14, 55128 Mainz (Germany)
E-mail: carsten.streb@uni-mainz.de

Prof. Dr. X. Chen
Green Catalysis Center and College of Chemistry, Zhengzhou University
Zhengzhou, 450001 (China)
E-mail: xuenian_chen@zzu.edu.cn

Introduction

The self-assembly of supramolecular aggregates from molecular building blocks provides a powerful strategy towards novel, functional nanostructures.[1–3] One particularly promising class of molecular components are molecular metal oxides, or polyoxometalates (POMs): POMs are anionic metal oxide clusters which bridge the gap between mononuclear metal oxo complexes and solid-state bulk metal oxides.[4,5] POMs feature unique properties such as tuneable structure and charge, high redox activity and unique acid-base chemistry, which has led to their application in fields ranging from catalysis[6,7] to bio-medicine.[8] However, due to the high symmetry of many classical POMs, their controlled and predictable assembly into supramolecular aggregates is difficult to achieve.

One approach to this end is the use of organo-functionalized POMs (organoPOMs) where the metal oxo cluster shell has been covalently functionalized with organic moieties.[9–11] Organo-functionalization provides control over the physical and electronic structure of the POMs, making them ideal building blocks for supramolecular assemblies.[12–14] Thus organoPOMs have successfully been employed as molecular components in the assembly of functional supramolecular systems with unique functions.[15]

Controlled aggregation of organoPOMs has been used to access a range of functional superstructures including vesicles, micelles, and hollow spheres, so-called blackberries.[12,16–18] Also, organo-functionalization of POMs with metal coordination sites (e.g., pyridines) has been used for the design of nanostructured organoPOM aggregates:[19–24] In one outstanding example, Izzet and colleagues described how Dawson-POMs can be covalently functionalized with terpyridine metal coordination sites. Binding of Fe^{2+} to these sites led to a hierarchical self-assembly, resulting in the formation of supramolecular triangles and nano-particles in the 6–10 nm range.[24]

An alternative approach towards supramolecular organoPOM aggregation is the use of non-covalent interactions. This has been successfully used to link organoPOMs to a range of functional systems including macrocycles,[25–27] biomolecules,[28–30] and carbon nanotubes[31,32] This strategy offers a broad scope, as the component combinations are almost unlimited.

To-date, most organoPOMs are based on triol-, imido-, organophosphorus-, organosilicon-, or organotin-linkages.[15,33] In contrast, the use of organoboronic acids as versatile and easily accessible organic linkage is still in its

infancy. Some of us have recently developed this field and demonstrated its use for designing supramolecular boronic acid-based organoPOM aggregates including several POM nanocapsules and a POM-boronic acid-polymer.[34–36]

Here, we aimed at extending this synthetic approach to the design of boronic acid-based organoPOM assemblies. To this end we were inspired by earlier studies which showed that lanthanide ions are ideally suited to link POMs into larger aggregates.[37–41]

Results and Discussion

In this work, four novel POM supramolecules (**Ln-POM**) were obtained by the reaction of 4-pyridinylboronic acid (4PyBA), Dawson anions $[P_2Nb_3W_{15}O_{62}]^{9-}$ (={Nb_3W_{15}}) and the corresponding lanthanide ions in water. The resulting title compounds are virtually isostructural with the general formula of $H_{27}[(4PyB)_3O_2(OH)_3][Ln_2(H_2O)_{12}(P_2Nb_3W_{15}O_{62})_4$-$(4PyBOH)_4]$ xH_2O (**Ln-POM**), (Ln=La^{3+} for **La-POM**, Ce^{3+} for **Ce-POM**, Pr^{3+} for **Pr-POM**, and Eu^{3+} for **Eu-POM**). These compounds were fully characterized by single-crystal and powder X-ray diffraction, elemental analyses, FTIR spectroscopy and thermogravimetric analysis, see Supporting Information for details.

The title compounds are composed of two components: the first component is a tetramer formed from four {Nb_3W_{15}} Dawson anions: two {Nb_3W_{15}} units are covalently linked by two 4PyBA units. Each boronic acid features one terminal –OH group and two B–O-Nb bridges which link the {Nb_3W_{15}} units (Figure 1a, and Supporting Information, Figure S1 and Table S2). The resulting POM dimers are then linked into tetramers by two Ln^{3+} cations which form Ln–O–W bonds between neighboring {Nb_3W_{15}} clusters, resulting in the species $[Ln_2(H_2O)_{12}(P_2Nb_3W_{15}O_{62})_4$-$(4PyBOH)_4]^{26-}$ (Ln=La, Ce, Pr, Eu), see Figure 1a. The second component is a T-shaped triboronate formed by condensation of three 4PyBAOH units, giving the species $[(4PyB)_3O_2(OH)_3]^-$, see Figure 1b. This species consists of three pyridine groups connected by a central {$B_3O_2(OH)$} ring (Figure 1b). In the crystal lattice, both components form infinite 1D chains where the POM tetramer and triboronates are linked non-covalently by a combination of π–π stacking, hydrogen bonding and electrostatic interactions, see Figures 1c and 1d for structural details. Bond valence sum (BVS) calculations (see SI, Table S2) indicated that the terminal oxygen atoms of the tetramer-based boronic acid, as well as three oxygen atoms in the triboronates are singly protonated, i.e., -OH groups (see Figure 1a,b, green spheres). All oxygen ligands on the Ln^{3+} ions were identified by BVS as coordinated water molecules (Figure 1a, light-blue spheres).

In the following, we will use **Ce-POM** as model for all **Ln-POMs** reported here. As shown in Figure 1e, the POM tetramers and the triboronates interact with each other through π–π stacking between neighboring pyridine ligands (centroid-to-centroid distance ca. 3.6 Å - 3.7 Å) and hydrogen bonding interactions between the POM tetramer and the triboronate (observed by short N···O distances between

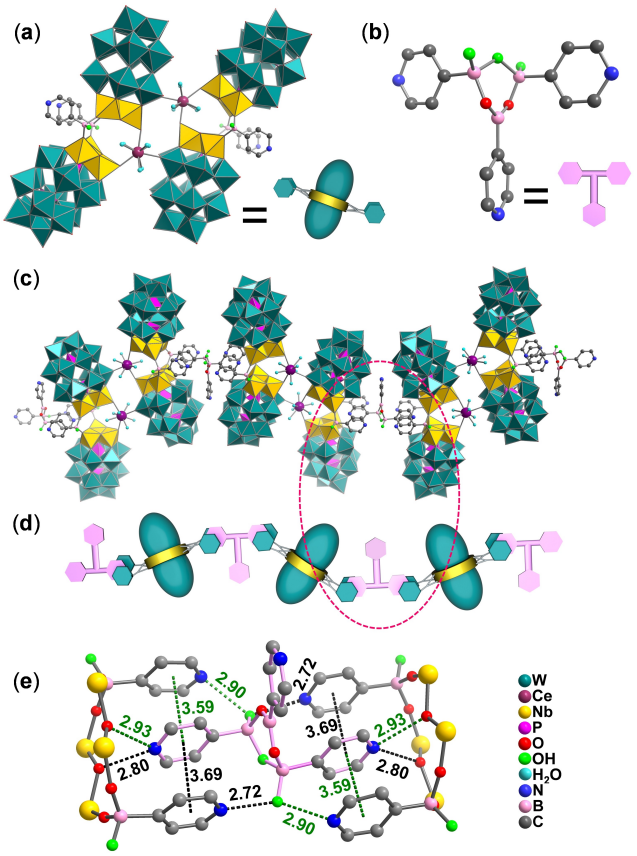

Figure 1. (a) Illustration of the tetrameric polyanion {[Ce-$(H_2O)_6]_2[P_2Nb_3W_{15}O_{62}]_4[4PyB(OH)]_4\}^{26-}$; (b) illustration of the T-shaped triboronate $[(4PyB)_3O_2(OH)_3]^-$; (c) illustration of the 1D supramolecular assembly of tetramers and triboronates; (d) simplified schematic diagram of the tetramer-triboronate assembly; (e) detailed illustration of the supramolecular interactions between the tetramer and triboronate components. All illustrations are based on single-crystal XRD data. H-atoms have been omitted for clarity.

2.7–2.9 Å). Note that these hydrogen-bonds involve the 3-pyridyl groups of the 4PyBA. These interactions might play a key role in forming the title compounds, as the use of the closely related 3-pyridyl boronic acid under similar conditions results in a strikingly different POM-organoboronic acid polymer.[35]

When exploring the principal properties of **Ce-POM**, we noted that crystalline particles of **Ce-POM** can easily be dispersed in anhydrous acetonitrile using ultrasonication for ≈6 h followed by centrifugation to remove large particles. This process results in a colloidal suspension ([**Ce-POM**] ≈0.165 mg/mL) which is stable under ambient conditions for more than one year and shows no indication of aggregation or precipitation. Scanning electron microscopy (SEM) of the isolated particles shows an average particle size of ≈45 nm, with a particle distribution range between ≈25 nm to 70 nm (Figures 2a,b). The colloids also show Tyndall scattering of red laser light (λ=650 nm, Figure 2b, inset). Dynamic light scattering (DLS) and Small-angle X-ray scattering (SAXS) measurements verified that the particle size and distribution is retained in the dispersed

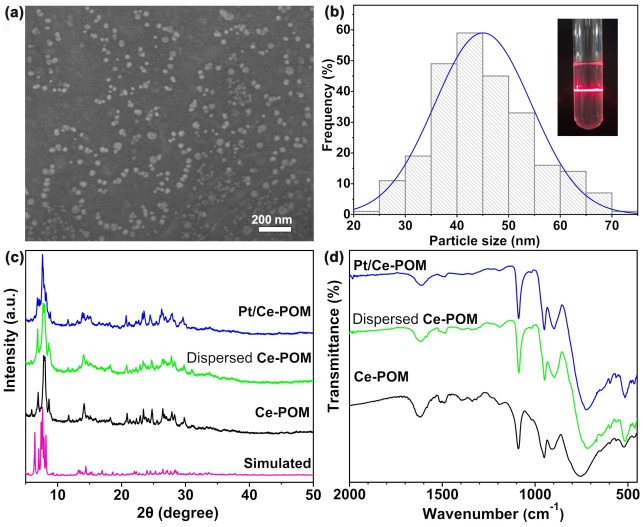

Figure 2. (a) SEM images and (b) particle size distribution of dispersed **Ce-POM** nanoparticles, (c) PXRD patterns and (d) IR spectra of **Ce-POM**, dispersed **Ce-POM** (recovered from acetonitrile) and **Pt/Ce-POM**.

phase and gave an average particle size of 61 nm and 46 nm respectively (Supporting Information, Figure S6 and S7). Powder X-ray diffraction (PXRD) and IR spectroscopy of the recovered **Ce-POM** particles (obtained by high-speed centrifugation from the colloidal suspension) indicate that the structure of **Ce-POM** is retained (Figures 2c,d).

We hypothesize that this facile dispersion of the compound might be related to the breaking of the weak intermolecular interactions in **Ce-POM**, similar to the top-down exfoliation used to access solid-state layered 2D materials.[42,43] For experimental details on colloid preparation and characterization, see SI.

Recent ground-breaking studies have highlighted the importance of metal-substrate interactions in catalysis. In particular for hydrogen activation, it has been demonstrated that the interplay between noble-metal particles (e.g., Pt) and catalyst supports (e.g., metal oxides) can lead to a so-called hydrogen spillover.[44,45] In hydrogen spillover, hydrogen atoms formed on the noble metal particle are transferred to the metal oxide support and can then be used for subsequent catalytic conversions. This phenomenon was first reported for Pt on WO_3,[46] so we hypothesized that the concept can possibly be transferred to polyoxotungstate clusters as catalyst supports also. This idea is inspired by recent seminal reports, where hydrogen spillover involving noble-metal-functionalized POMs has been used: Yan and co-workers studied hydrogen spillover in the molecular POM-single-atom catalyst (POM-SAC)[47] $[PdPMo_{11}O_{39}]^{5-}$ and demonstrated high thermal reduction catalysis, e.g., for C=O and nitro group reduction.[48] Yamaguchi, Suzuki and co-workers used mixed-valent $\{Ag^{I/0}{}_n\}$ clusters stabilized by polyoxotungstates to model processes related to hydrogen spillover:[49,50] reaction of the species with H_2 led to the storage of electrons on the $\{Ag_n\}$ clusters, while the protons were transferred to the polyoxotungstate shell. These studies were focused on designing molecular models for H_2 activation, while to the best of our knowledge, POMs have thus far not been used as heterogeneous molecular metal oxide supports for noble-metal catalysts in hydrogen spillover.

Inspired by these studies, we have explored how the colloidal **Ce-POM** particles can be used as heterogeneous support for Pt catalyst particles. To this end, a suspension of **Ce-POM** was surface-modified with Pt by UV-photochemical reduction. To this end, a chloroplatinic acid solution containing **Ce-POM** colloidal particles in acetonitrile/ethanol was irradiated with UV-light, resulting in the formation of **Pt/Ce-POM** (for synthetic details see Supporting Information). Transmission electron microscopy (TEM) images show that crystalline Pt nanoparticles (Pt NPs, average size $\approx$3 nm) are uniformly dispersed on the surface of the larger **Ce-POM** particles (Figure 3a,b and Supporting Information, Figure S11). High-resolution TEM indicated lattice fringes (lattice spacing = 0.23 nm) which correspond to the (111) plane of metallic Pt. Note that due to the low Pt content, no diffraction peaks from Pt particles could be observed by PXRD analysis.

A striking first indication for a possible hydrogen spillover in **Pt/Ce-POM** was obtained when exposing the sample to gaseous H_2 (1 bar) at room temperature, which resulted in the instantaneous colour change from pale-yellow to deep blue (Supporting Information, Figure S14 and Supporting Video file). This is indicative of the formation of reduced, mixed-valent tungsten oxide-based systems, where the characteristic blue color is due to intervalence charge-transfer (IVTC) transitions between W^V and W^{VI} centers.[51] Note that this tungsten reduction is reversible: when exposed to air, the sample returns to its original colour within approximately six minutes.

X-ray photoelectron spectroscopy (XPS) was used to gain in-depth understanding of the processes occurring during the reaction of **Pt/Ce-POM** with gaseous H_2. XPS of the native **Pt/Ce-POM** verifies that all W centers are present as W^{6+} (binding energies: 35.95 eV for W $4f_{7/2}$ and 38.05 eV for W $4f_{5/2}$, Figure 4a), while the deconvoluted Pt spectrum indicates the presence of mixed-valent species, Pt^0 (71.7 eV and 74.9 eV) and Pt^{2+} (73.44 eV and 76.60 eV) for Pt $4f_{7/2}$ and Pt $4f_{5/2}$ respectively (Figure 4b). These results suggest

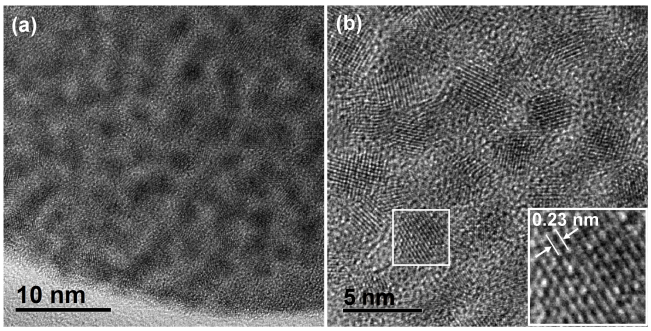

Figure 3. (a) and (b) TEM images of Pt NPs on **Pt/Ce-POM** at different magnifications. Inset: high-resolution TEM of the crystalline lattice observed.

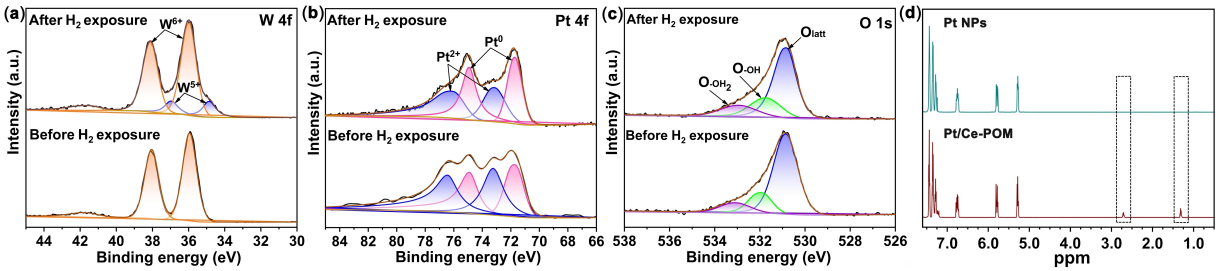

Figure 4. (a) - (c) deconvoluted XPS data for **Pt/Ce-POM** before and after exposure to H_2: (a) W 4f, (b) Pt 4f, (c) O 1s. (d) ^{1}H NMR spectra of the reaction of phenylethylene with **Pt/Ce-POM** and a **Pt NPs** reference after hydrogen spillover and replacing the residual H_2 with Argon.

that surface Pt centers in **Pt/Ce-POM** were partially oxidized when exposed to ambient atmosphere during sample preparation and handling. The positive shift of the binding energy (BE) of Pt in **Pt/Ce-POM** compared with bulk Pt metal (71.3 eV for Pt $4f_{7/2}$)[52] is probably due to catalyst/support interactions between **Ce-POM** and Pt.[53]

As shown in Figure 4 and Supporting Information, Table S3, reaction of **Pt/Ce-POM** with H_2, leads to a partial reduction of the W^{6+} centers to W^{5+} (characteristic BE: 34.86 eV and 36.90 eV). From XPS deconvolution, we can estimate the reduction degree to ≈15.9 atom-%. Comparison of the deconvoluted O 1s XPS data shows that upon H_2 exposure, the amount of protonated oxygen groups (i.e., –OH and $–OH_2$) increases from 26.9 atom-% to 39.4 atom-% (Figure 4c and Supporting Information, Table S3). These data suggest that reaction of H_2 with **Pt/Ce-POM** leads to a hydrogen spillover where molecular H_2 is dissociated by Pt and retained as protons (stored by protonation of the POM) and electrons (stored as reduced W^{5+} atoms of the POM). Furthermore, after H_2 exposure, the amount of Pt^0 in **Pt/Ce-POM** increased, and the Pt^0 : Pt^{2+} molar ratio changed from 1:1.2 to 1:0.89, indicating that part of the surface Pt^{2+} was reduced.

Based on this insight, and inspired by earlier works on Pt-on-tungsten oxide hydrogen spillover catalysts,[45,46] we decided to investigate the catalytic performance of **Pt/Ce-POM** for selected model hydrogenations under mild conditions (1 bar H_2, room temperature). Based on initial optimization reactions (details see Supporting Information, Table S4) we could show that **Pt/Ce-POM** efficiently catalyzes the hydrogenation of aliphatic and aromatic olefins to the corresponding alkanes. Full conversion is observed in most cases within 15 min reaction time at room temperature and 1 bar H_2 using 0.5 mol-% of **Pt/Ce-POM** (calculated based on Pt content, see Figure 5).

To gain further insights into the reaction mechanism, a set of control experiments was conducted using styrene as the model substrate (Table 1). In the absence of any catalyst, or when using the non-Pt-decorated **Ce-POM**, no phenylethylene can be detected (entry 1). When using commercial **Pt NPs** (entry 2) or a physical mixture of **Pt NPs** and **Ce-POM** (entry 3), only low conversion (<20 %) is observed, which indicates that the two components in **Pt/Ce-POM** act in a synergistic fashion, as proposed by the hydrogen spillover mechanism. Both **Pt/Ce-POM** and **Pt/La-POM**

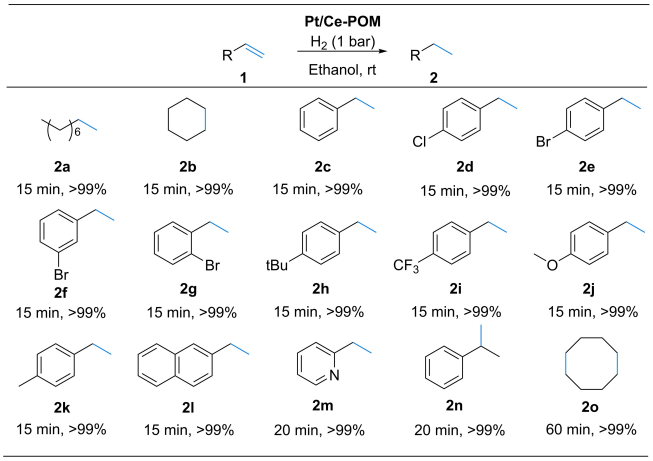

Figure 5. Hydrogenation of olefins to the corresponding alkanes catalyzed by **Pt/Ce-POM**. Reaction conditions: substrate (0.5 mmol), **Pt/Ce-POM** (0.5 mol % with respect to the substrate, based on Pt), EtOH (2 mL), r.t., H_2 (1 bar, H_2 balloon). Yields were determined by GC-MS.

Table 1: Control experiments for the styrene hydrogenation.[a]

Entry	Catalyst	Yield [%][b]
1	**Ce-POM**[c]	–
2	**Pt NPs**[d]	15.4
3	**Pt NPs** + **Ce-POM**[c]	19.6
4	**Pt/La-POM**	>99
5	**Pt/Ce-POM**	>99
6[e]	**Pt/Ce-POM** or **Pt NPs, no H_2**	–

[a] Reaction conditions: styrene (0.5 mmol), catalyst (0.5 mol % based on Pt), ethanol (2 mL), reaction time: 15 min; [b] yields determined by GC-MS; [c] amount of **Ce-POM** identical to the amount of **Ce-POM** in the **Pt/Ce-POM** experiment, entry 5; [d] commercial **Pt NPs**, particle size 10 nm, [e] without H_2.

show high catalytic efficiency with complete conversion, suggesting that the type of lanthanide ion present in the catalyst does not affect the catalytic performance (entries 4 and 5). Without H_2, neither **Pt/Ce-POM** nor **Pt NPs** catalyze the conversion of styrene, which indicates that H_2 is essential as the reducing agent, i.e., proton and electron donor (entry 6).

To understand whether the **Ce-POM** is actively involved in the olefin hydrogenation reaction, the following ^{1}H NMR

spectroscopic control experiments were performed. First, we performed the standard hydrogen spillover experiment for **Pt/Ce-POM** and **Pt NPs** (as reference). Upon reduction of the **Pt/Ce-POM**, the excess gaseous H_2 was removed by purging with Argon. Then, styrene was injected into the reaction vessel and the reaction was followed by ^{1}H NMR, for experimental details see Supporting Information, Figure S16). As shown in Figure 4d, ^{1}H NMR spectroscopy shows that styrene is only hydrogenated by **Pt/Ce-POM**, while no hydrogenation is observed for the **Pt NP** reference. This indicates that styrene reduction involves the **Ce-POM**, and suggests that the protons and electrons stored on the **Ce-POM** are used for olefin hydrogenation. Also, we note that the Pt particles are distributed uniformly across the external surface of the **Ce-POM**. This is expected to facilitate access to Pt–H species by the substrate to allow direct H transfer during the olefin hydrogenation.[48]

Recycling experiments show that the hydrogenation performance of **Pt/Ce-POM** was retained over five runs (Supporting Information, Figure S17). Further, IR spectroscopy and PXRD of **Pt/Ce-POM** before and after the five catalytic runs confirm the stability of the material under the catalytic conditions employed (Supporting Information, Figure S18).

To investigate the scope of this process, we examined the catalytic activity of **Pt/Ce-POM** for the hydrogenation of nitrobenzene and carbonyl derivatives. As shown in the Supporting Information, Table S6, **Pt/Ce-POM** catalyzes the full conversion of most nitrobenzene derivatives studied to the corresponding amines within 30 min at room temperature and 1 bar H_2. Note that **Pt/Ce-POM** does not catalyse carbonyl hydrogenation under the mild conditions used. As shown in the Supporting Information, Table S8, when various aldehydes or ketones were used as substrates, no hydrogenation products (i.e., alcohols) were detected in acetonitrile as solvent, and only very low amounts were observed in ethanol as solvent. We suggest that this selective hydrogenation behaviour is related to the differences in electron deficiency of the nitro- and carbonyl-compounds, which is expected to lead to different interactions between the substrate and **Pt/Ce-POM**.[54] Also note that acetals were formed as side-products by reaction of the carbonyls with the ethanol solvent. We propose that this reaction was triggered by acid catalysis by **Pt/Ce-POM**.

Conclusion

In summary, a family of unprecedented boronic acid-POMs supramolecular assemblies are reported where weak intermolecular interactions facilitate the formation of stable colloidal suspensions. Loading of these aggregates with Pt particles results in high-performance hydrogenation catalysts which are considered to operate via a hydrogen spillover mechanism, see Figure 6. Initial mechanistic studies show that the title POMs play a key role as electron and proton reservoirs in the hydrogenation. The new concept presented in this study can trigger the development of new classes of technologically important catalysts, e.g., for the environmentally friendly production of fine-chemicals or pharmaceuticals. Future work will focus on mechanistic understanding of the structural and electronic linkage of Pt and **Ce-POM** particles as well as the atomic-level mechanism of hydrogen spillover to facilitate the observed hydrogenation reactivity.

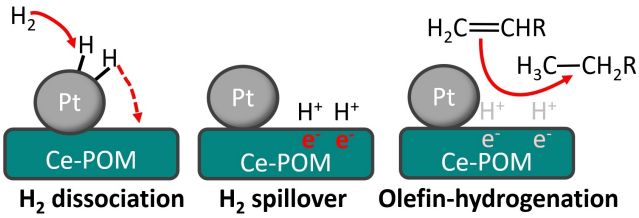

Figure 6. Schematic illustration of the proposed hydrogenation mechanism by **Pt/Ce-POM**.

Acknowledgements

This work was supported by the National Natural Science Foundation of China (22171073 and 22171246), the Program for Science & Technology Innovation Talents in Universities of Henan Province (23HASTIT005). C.S. gratefully acknowledges support by Johannes Gutenberg University Mainz, the Gutenberg Research College Mainz, the Rheinland-Pfalz Research Initiative through the Top-Level Research Area "SusInnoScience", and the Deutsche Forschungsgemeinschaft DFG (TRR 234, CataLight, project no: 364549901, project A4). This work contributes to the DFG SFB Initiative SFB 1633 "PCET". Open Access funding enabled and organized by Projekt DEAL.

Conflict of Interest

The authors declare no conflict of interest.

Data Availability Statement

The data that support the findings of this study are available from the corresponding author upon reasonable request.

Keywords: Boronic Acid · Hydrogen Spillover · Polyoxometalate · Self-Assembly · Supramolecular

[1] F. Freire, E. Quiñoá, R. Riguera, *Chem. Rev.* **2016**, *116*, 1242–1271.
[2] K. Sato, M. P. Hendricks, L. C. Palmer, S. I. Stupp, *Chem. Soc. Rev.* **2018**, *47*, 7539–7551.
[3] Q. Liu, X. Wang, *Angew. Chem. Int. Ed.* **2023**, *62*, e202217764.
[4] M. T. Pope, A. Müller, *Angew. Chem. Int. Ed.* **1991**, *30*, 34–48.
[5] L. Cronin, A. Müller, *Chem. Soc. Rev.* **2012**, *41*, 7333–7334.
[6] I. A. Weinstock, R. E. Schreiber, R. Neumann, *Chem. Rev.* **2018**, *118*, 2680–2717.
[7] S.-S. Wang, G.-Y. Yang, *Chem. Rev.* **2015**, *115*, 4893–4962.

[8] F. de Azambuja, J. Moons, T. N. Parac-Vogt, *Acc. Chem. Res.* **2021**, *54*, 1673–1684.
[9] A. Proust, B. Matt, R. Villanneau, G. Guillemot, P. Gouzerha, G. Izzet, *Chem. Soc. Rev.* **2012**, *41*, 7605–7622.
[10] A. V. Anyushin, A. Kondinski, T. N. Parac-Vogt, *Chem. Soc. Rev.* **2020**, *49*, 382–432.
[11] D. Pakulski, A. Gorczyński, D. Brykczyńska, V. Montes-García, W. Czepa, I. Janica, M. Bielejewski, M. Kubicki, V. Patroniak, P. Samorì, A. Ciesielski, *Angew. Chem. Int. Ed.* **2023**, *62*, e202305239.
[12] P. Yin, D. Li, T. Liu, *Chem. Soc. Rev.* **2012**, *41*, 7368–7383.
[13] M. Stuckart, K. Y. Monakhov, *Chem. Sci.* **2019**, *10*, 4364–4376.
[14] B. Li, L. Xuan, L. Wu, *Macromol. Rapid Commun.* **2022**, *43*, 2200019.
[15] J. M. Cameron, G. Guillemot, T. Galambos, S. S. Amin, E. Hampson, K. Mall Haidaraly, G. N. Newton, G. Izzet, *Chem. Soc. Rev.* **2022**, *51*, 293–328.
[16] S. Polarz, S. Landsmann, A. Klaiber, *Angew. Chem. Int. Ed.* **2014**, *53*, 946–954.
[17] E. Hampson, J. M. Cameron, S. Amin, J. Kyo, J. A. Watts, H. Oshio, G. N. Newton, *Angew. Chem. Int. Ed.* **2019**, *58*, 18281–18285.
[18] C. P. Pradeep, M. F. Misdrahi, F.-Y. Li, J. Zhang, L. Xu, D.-L. Long, T. Liu, L. Cronin, *Angew. Chem. Int. Ed.* **2009**, *48*, 8309–8313.
[19] E. Hampson, J. M. Cameron, J. A. Watts, G. N. Newton, *Chem. Commun.* **2020**, *56*, 8237–8240.
[20] J. Yan, H. Huang, Z. Miao, Q. Zhang, Y. Yan, *Macromolecules* **2019**, *52*, 9545–9554.
[21] C. Martin, K. Kastner, J. M. Cameron, E. Hampson, J. Alves Fernandes, E. K. Gibson, D. A. Walsh, V. Sans, G. N. Newton, *Angew. Chem. Int. Ed.* **2020**, *59*, 14331–14335.
[22] X.-X. Li, Y.-X. Wang, R.-H. Wang, C.-Y. Cui, C.-B. Tian, G.-Y. Yang, *Angew. Chem. Int. Ed.* **2016**, *55*, 6462–6466.
[23] Y. Zhu, P. Yin, F. Xiao, D. Li, E. Bitterlich, Z. Xiao, J. Zhang, J. Hao, T. Liu, Y. Wang, Y. Wei, *J. Am. Chem. Soc.* **2013**, *135*, 17155–17160.
[24] G. Izzet, B. Abécassis, D. Brouri, M. Piot, B. Matt, S. A. Serapian, C. Bo, A. Proust, *J. Am. Chem. Soc.* **2016**, *138*, 5093–5099.
[25] W. Guan, G. Wang, J. Ding, B. Li, L. Wu, *Chem. Commun.* **2019**, *55*, 10788–10791.
[26] G. Izzet, M. Ménand, B. Matt, S. Renaudineau, L.-M. Chamoreau, M. Sollogoub, A. Proust, *Angew. Chem. Int. Ed.* **2012**, *51*, 487–490.
[27] B. Zhang, L. Yue, Y. Wang, Y. Yang, L. Wu, *Chem. Commun.* **2014**, *50*, 10823–10826.
[28] B. M. Čolović, M. Lacković, J. Lalatović, S. A. Mougharbel, U. Kortz, Z. D. Krstić, *Curr. Med. Chem.* **2020**, *27*, 362–379.
[29] A. Blazevic, A. Rompel, *Coord. Chem. Rev.* **2016**, *307*, 42–64.
[30] C. Molitor, A. Bijelic, A. Rompel, *Chem. Commun.* **2016**, *52*, 12286–12289.
[31] D. Ma, L. Liang, W. Chen, H. Liu, Y.-F. Song, *Adv. Funct. Mater.* **2013**, *23*, 6100–6105.
[32] C. Bosch-Navarro, B. Matt, G. Izzet, C. Romero-Nieto, K. Dirian, A. Raya, S. I. Molina, A. Proust, D. M. Guldi, C. Martí-Gastaldo, E. Coronado, *Chem. Sci.* **2014**, *5*, 4346–4354.
[33] A. Dolbecq, E. Dumas, C. R. Mayer, P. Mialane, *Chem. Rev.* **2010**, *110*, 2680–2717.
[34] S. Li, Y. Zhou, N. Ma, J. Zhang, Z. Zheng, C. Streb, X. Chen, *Angew. Chem. Int. Ed.* **2020**, *59*, 8537–8540.
[35] S. Li, Y. Zhao, S. Knoll, R. Liu, G. Li, Q. Peng, P. Qiu, D. He, C. Streb, X. Chen, *Angew. Chem. Int. Ed.* **2021**, *60*, 16953–16957.
[36] S. Li, Y. Zhao, H. Qi, Y. Zhou, S. Liu, X. Ma, J. Zhang, X. Chen, *Chem. Commun.* **2019**, *55*, 2525–2528.
[37] M. Sadakane, M. H. Dickman, M. T. Pope, *Angew. Chem. Int. Ed.* **2000**, *39*, 2914–2916.
[38] J. C. Liu, Q. Han, L. J. Chen, J. W. Zhao, C. Streb, Y. F. Song, *Angew. Chem. Int. Ed.* **2018**, *57*, 8416–8420.
[39] F. Hussain, F. Conrad, G. R. Patzke, *Angew. Chem. Int. Ed.* **2009**, *48*, 9088–9091.
[40] B. S. Bassil, M. H. Dickman, I. Römer, B. von der Kammer, U. Kortz, *Angew. Chem. Int. Ed.* **2007**, *46*, 6192–6195.
[41] J.-C. Liu, J.-W. Zhao, C. Streb, Y.-F. Song, *Coord. Chem. Rev.* **2022**, *471*, 214734.
[42] T.-H. Le, Y. Oh, H. Kim, H. Yoon, *Chem. Eur. J.* **2020**, *26*, 6360–6401.
[43] V. Nicolosi, M. Chhowalla, M. G. Kanatzidis, M. S. Strano, J. N. Coleman, *Science* **2013**, *340*, 1226419.
[44] W. Karim, C. Spreafico, A. Kleibert, J. Gobrecht, J. Vandevondele, Y. Ekinci, J. A. van Bokhoven, *Nature* **2017**, *541*, 7635.
[45] R. Prins, *Chem. Rev.* **2012**, *112*, 2714–2738.
[46] S. Khoobiar, *J. Phys. Chem.* **1964**, *68*, 411–412.
[47] R. Liu, C. Streb, *Adv. Energy Mater.* **2021**, *11*, 2101120.
[48] M. J. Hülsey, V. Fung, X. Hou, J. Wu, N. Yan, *Angew. Chem. Int. Ed.* **2022**, *61*, e202208237.
[49] K. Yonesato, S. Yamazoe, D. Yokogawa, K. Yamaguchi, K. Suzuki, *Angew. Chem. Int. Ed.* **2021**, *60*, 16994–16998.
[50] K. Yonesato, D. Yanai, S. Yamazoe, D. Yokogawa, T. Kikuchi, K. Yamaguchi, K. Suzuki, *Nat. Chem.* **2023**, *15*, 940.
[51] C. Streb, *Dalton Trans.* **2012**, *41*, 1651–1659.
[52] S. Hüfner, G. K. Wertheim, *Phys. Rev. B* **1975**, *11*, 678–683.
[53] Y. Li, Y. Zhang, K. Qian, W. Huang, *ACS Catal.* **2022**, *12*, 1268–1287.
[54] L. Zhang, M. Zhou, A. Wang, T. Zhang, *Chem. Rev.* **2020**, *120*, 683–733.

Manuscript received: October 6, 2023
Accepted manuscript online: October 27, 2023
Version of record online: ■■, ■■

Research Articles

Polyoxometalates

S. Li,* Y. Ma, Y. Zhao, R. Liu, Y. Zhao,
X. Dai, N. Ma, C. Streb,*
X. Chen* _____ **e202314999**

Hydrogenation Catalysis by Hydrogen Spillover on Platinum-Functionalized Heterogeneous Boronic Acid-Polyoxometalates

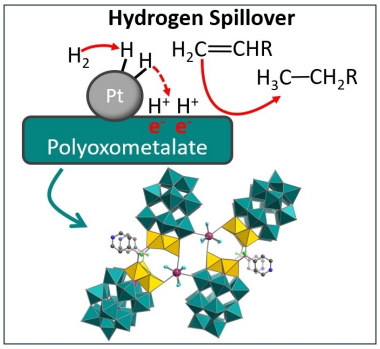

Supramolecular colloids based on polyoxometalates functionalized with boronic acids are modified with Pt particles to yield high-performance hydrogenation catalysts. Mechanistic studies reveal that the systems operate by a hydrogen spillover mechanism, enabling efficient hydrogenation of olefins to alkanes and nitroarenes to amines under mild conditions.